Journal of Power Sources 189 (2009) 365–370

Contents lists available at ScienceDirect

Journal of Power Sources

journal homepage: www.elsevier.com/locate/jpowsour

Li-ion transport in all-solid-state lithium batteries with $LiCoO_2$ using NASICON-type glass ceramic electrolytes

J. Xie, N. Imanishi, T. Zhang, A. Hirano, Y. Takeda*, O. Yamamoto

Department of Chemistry, Faculty of Engineering, Mie University, 1577 Kurimamachiya-cho, Tsu, Mie 514-8507, Japan

ARTICLE INFO

Article history:
Received 16 June 2008
Received in revised form 9 July 2008
Accepted 8 August 2008
Available online 19 August 2008

Keywords:
All-solid-state batteries
Solid electrolyte/$LiCoO_2$ interface
Chemical diffusion coefficient
Potentiostatic intermittent titration technique
Electrochemical impedance spectroscopy

ABSTRACT

$LiCoO_2$ thin films were deposited on the NASICON-type glass ceramics, $Li_{1+x+y}Al_xTi_{2-x}Si_yP_{3-y}O_{12}$, by radio frequency (RF) magnetron sputtering and were annealed at different temperatures. The as-deposited and the annealed $LiCoO_2$ thin films were characterized by X-ray diffraction (XRD), Raman spectroscopy and scanning electron microscopy (SEM). It was found that the films exhibited a (1 0 4) preferred orientation after annealing and Co_3O_4 was observed by annealing over 500 °C due to the reaction between the $LiCoO_2$ and the glass ceramics. The effect of annealing temperature on the interfacial resistance of glass ceramics/$LiCoO_2$ and Li-ion transport in the bulk $LiCoO_2$ thin film was investigated by galvanostatic cycling, cyclic voltammetry (CV), potentiostatic intermittent titration technique (PITT) and electrochemical impedance spectroscopy (EIS) with the Li/PEO/glass ceramics/$LiCoO_2$ cell. The cell performance was limited by the Li-ion diffusion resistance in Ohara/$LiCoO_2$ interface as well as in bulk $LiCoO_2$.

1. Introduction

In recent years, all-solid-state thin-film Li-ion batteries have received much interest due to their potential application in microdevices. A solid electrolyte with a high Li-ion conductivity is essential to fabricate practical all-solid-state Li-ion batteries. Recently, the NASICON-type Li-ion conducting electrolyte consisted of Li_2O–Al_2O_3–SiO_2–P_2O_5–TiO_2 has received great attention because of its high Li-ion conductivity of $10^{-4} \sim 10^{-3}$ S cm^{-1} at room temperature [1,2]. Birke et al. [3] successfully cycled the all-solid-state $Li_4Ti_5O_{12}/Li_{1.3}Al_{0.3}Ti_{1.7}(PO_4)_3/LiMn_2O_4$ cell which exhibited a charge–discharge plateau at around 2.5 V. Inda et al. [4] also reported the all-solid-state $Li_4Ti_5O_{12}$/composite electrolyte/$LiCoO_2$ cell which showed good charge–discharge performance. The composite electrolyte was composed of NASICON-type glass ceramics and ployethyleneoxide (PEO)-based polymer electrolyte. In both cases, composite electrodes were used. Iriyama et al. [5] fabricated the all-solid-state thin-film Li-ion cell using the NASICON-type solid electrolyte and the pulsed laser deposited amorphous Li–Mn–O film cathode. Generally, it is necessary to anneal the thin film at high temperature in order to achieve good electrochemical performance of the batteries. Thus, the chemical stability of the electrode materials toward electrolyte is rather important.

It was reported that some electrode materials, such as $LiMn_2O_4$ (up to 600 °C) [6], $Li_4Ti_5O_{12}$ (up to 600 °C) [7], $LiCoPO_4$ and $Li_3Fe_2(PO_4)_3$ (up to 900–1000 °C) [8], showed chemical stability toward NASICON-type solid electrolyte. By contrast, Nakata and Nanno [8] observed obvious reaction between the electrolyte and $LiCoO_2$ at 900–1000 °C. Therefore, it is important to clarify the reaction mechanism and its effect on the electrochemical performance of $LiCoO_2$-based thin-film Li-ion batteries with the NASICON-type solid electrolyte. In our present work, $LiCoO_2$ thin films were deposited on the NASICON-type solid electrolyte by radio frequency (RF) magnetron sputtering, and the interfacial stability at elevated temperature was investigated by X-ray diffraction (XRD) and Raman spectroscopy. The interfacial resistance of solid electrolyte/$LiCoO_2$ and the Li-ion diffusion in $LiCoO_2$ were evaluated by electrochemical impedance spectroscopy (EIS) and potentiostatic intermittent titration technique (PITT) using the Li/PEO/glass ceramics/$LiCoO_2$ cell.

2. Experimental

The glass ceramics plates, $Li_{1+x+y}Al_xTi_{2-x}Si_yP_{3-y}O_{12}$, provided by OHARA Inc. (0.15 mm in thickness) were used as the solid electrolyte for the following experiments. The glass ceramics is named Ohara in the following paragraphs. $LiCoO_2$

* Corresponding author. Tel.: +81 59 231 9421; fax: +81 59 231 9419.
E-mail address: takeda@chem.mie-u.ac.jp (Y. Takeda).

0378-7753/$ – see front matter © 2008 Elsevier B.V. All rights reserved.
doi:10.1016/j.jpowsour.2008.08.015

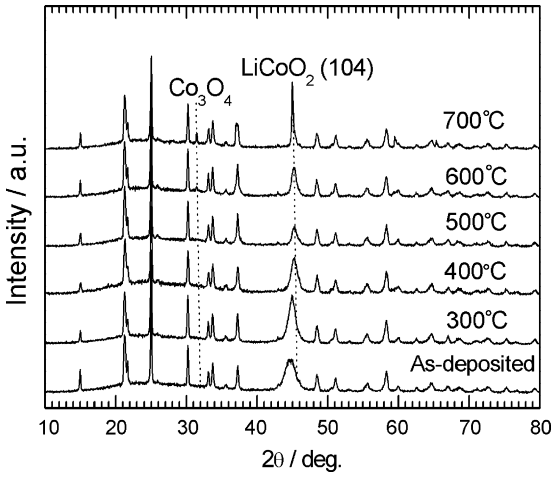

Fig. 1. XRD patterns of $LiCoO_2$ thin films on Ohara annealed at different temperatures.

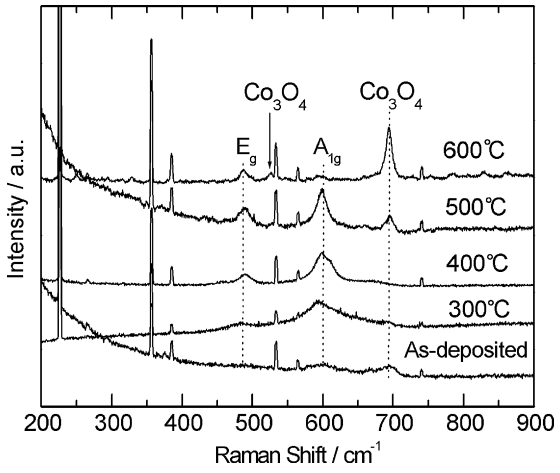

Fig. 2. Raman spectra of $LiCoO_2$ thin films on Ohara annealed at different temperatures.

thin films (8 mm × 8 mm) were deposited on Ohara substrates (10 mm × 10 mm) by RF magnetron sputtering using a Ulvac SCOTT-C3. The sputtering of $LiCoO_2$ was carried out in pure Ar with a working pressure of 2 Pa and a sputtering power of 50 W. The thickness of the film was about 0.8 μm for 2 h sputtering. The as-deposited $LiCoO_2$ thin films were annealed at 300–700 °C for 30 min in air to improve crystallization. The crystal structure of the sputtered $LiCoO_2$ thin film was characterized by XRD using a RINT2000/PC diffractometer with Cu Kα radiation and by Raman spectroscopy using a RNANOD T64000M1. The cross-section morphology of the films was observed by scanning electron microscopy (SEM) using a Hitachi S-4000. The Li/PEO_{18}–Li$(CF_3SO_2)_2$N/Ohara/$LiCoO_2$ cells were fabricated to investigate the interfacial resistance of Ohara/$LiCoO_2$ and Li-ion chemical diffusion coefficient in $LiCoO_2$. Au was sputtered on the surface of $LiCoO_2$ thin film as the current collection. To prevent the reaction between Li and Ohara, the PEO based solid polymer film (PEO_{18}-Li$(CF_3SO_2)_2$N, abbreviated as PEO) was inserted between them. The polymer electrolyte was prepared using our previously reported method [9]. The electrochemical performance of the all-solid-state cells was characterized by galvanostatic cycling at 10 μA between 3 and 4.3 V and cyclic voltammetry (CV) at a scanning rate 0.2 mV s^{-1}. Li-ion transfer resistance through Ohara/$LiCoO_2$ interface was measured by EIS. Li-ion chemical diffusion coefficient in $LiCoO_2$ bulk was measured by PITT and EIS. The detailed measurement method was described elsewhere [10,11]. All the above electrochemical measurements were performed at 50 °C. To see the interfacial resistances of Li/PEO, PEO/Ohara, and Ohara/$LiCoO_2$ in the Li/PEO/Ohara/$LiCoO_2$ cell, symmetric cells Li/PEO/Li, Au/PEO/Au, Au/Ohara/Au, Li/PEO/Ohara/PEO/Li and Au/$LiCoO_2$/Ohara/$LiCoO_2$/Au were fabricated and characterized by EIS in at 5–80 °C. The EIS measurements were carried out by applying an AC signal of 10 mV amplitude over the frequency range from 1 MHz to 1 mHz using a Solartron 1287 electrochemical interface combined with a Solartron 1260 frequency response analyzer.

3. Results and discussion

Fig. 1 shows the XRD patterns of $LiCoO_2$ thin films sputtered on Ohara annealed at various temperatures. It can be seen that the as-prepared $LiCoO_2$ thin film is not well crystallized evidenced by a broad peak located 45°. Note that, with increasing annealing temperatures, the broad peak become sharp with its position shifted to a high angle. It is clear that $LiCoO_2$ thin films on Ohara crystallized with a (1 0 4) preferred orientation. Similar orientation was also observed for the 1.35 μm thick $LiCoO_2$ thin film on Au substrate in our previous work [10]. The (1 0 4) preferred orientation is favorable for the rapid Li-ion diffusion through the $LiCoO_2$ lattice, because the Li layers lie parallel to the direction of the diffusion for this orientation. When the film was annealed at 600 °C for 30 min, a small peak appears at around 31°, which suggests reaction between $LiCoO_2$ and Ohara. The intensity of the additional peak increases with increasing annealing temperature. The XRD pattern suggests the presence of Co_3O_4.

Raman spectra of the $LiCoO_2$ thin films on Ohara annealed at various temperatures gave clearer results for the reaction between $LiCoO_2$ and Ohara as shown in Fig. 2. Tow peaks located at around 490 and 600 cm^{-1} correspond to O–Co–O bending mode (E_g) and Co–O stretching mode (A_{1g}), respectively, which are typical of the high temperature hexagonal $LiCoO_2$ phase. The peaks at around 520 and 700 cm^{-1} are attributed to Co_3O_4 [12–14]. Note that, Co_3O_4 is formed at 500 °C and the formation of Co_3O_4 becomes significant at 600 °C.

Fig. 3 shows the cross-sectional SEM images of $LiCoO_2$ thin films sputtered on Ohara substrates. The thickness of the film is about 0.8 μm. According to the weight gain of the sputtered film and the observed thickness, the compactness of the film is estimated to be about 90%. Note that the film is homogeneous and crack free and it becomes compact after annealing at 400 °C.

The cell performance of the all-solid-state lithium secondary cell with Ohara electrolyte, Li anode, and $LiCoO_2$ cathode was examined. The NASICON-type glass ceramics is chemically unstable with the direct contact with Li metal. Therefore, the PEO based electrolyte, PEO_{18}-Li$(CF_3SO_2)_2$N, was used as the interface protecting layer between Li and Ohara. The ion conductivity of PEO is too low to pass a high current at room temperature. Therefore, the electrochemical performance was obtained at 50 °C. Fig. 4 shows the Nyquist plots of freshly assembled Li/PEO/Ohara/$LiCoO_2$ cells at 50 °C. The cell resistance depends on the annealing temperature as seen in Fig. 4. The impedance profiles show two semicircles in a high and medium-frequency range followed by a sloping line in a low-frequency range. The diameter of medium-frequency semicircle increases with increasing annealing temperature. It means that this semicircle corresponds to the Ohara/$LiCoO_2$ interface. The high interfacial resistance for the 500 °C annealed Ohara/$LiCoO_2$ could be explained by the formation of Co_3O_4. The diameter of the high-frequency semicircle shows no dependence on the annealing temperature.

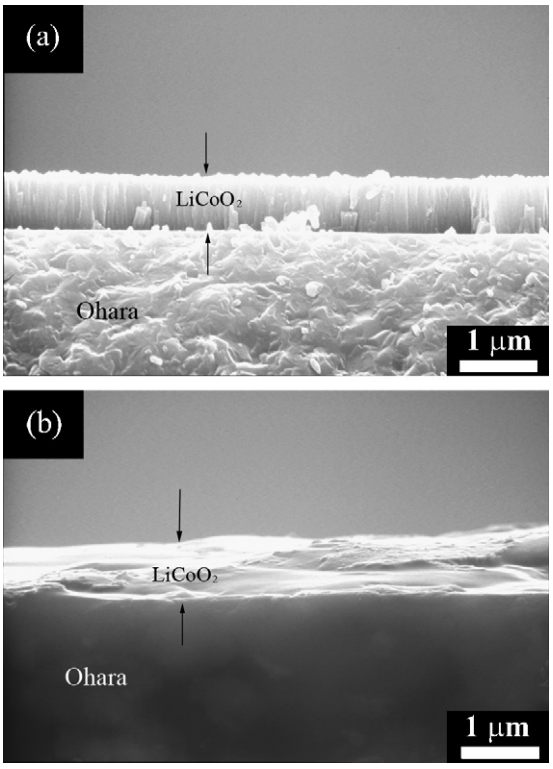

Fig. 3. Cross-sectional SEM images of the $LiCoO_2$ thin films on Ohara: (a) as-deposited and (b) annealed at 400 °C.

Fig. 5 shows the charge and discharge curves of the Li/PEO/Ohara/$LiCoO_2$ cells at 50 °C as a function of the annealing temperature of Ohara/$LiCoO_2$. The as-deposited $LiCoO_2$ shows a high capacity of 180 mAh g^{-1}, corresponding to an extraction of 0.64 Li from $LiCoO_2$, which is a little higher than that observed for the $LiCoO_2$ cathode with liquid electrolytes. The high capacity may be due to a low estimation of the $LiCoO_2$ mass or a high charge potential. The capacity of the cell decreases by annealing the Ohara/$LiCoO_2$ couple. It could be explained by the increasing cell resistance as shown in Fig. 4.

To analyze which side of the interface shows the dominant resistance, the cell resistances of the Li/PEO/Ohara/PEO/Li and Li/PEO/Li cells were examined with the help of the impedance analysis. Fig. 6 shows the impedance profiles of the Li/PEO/Li and Li/PEO/Ohara/PEO/Li cells at room temperature and 50 °C. At room temperature, two clear semicircles are formed in both the cells.

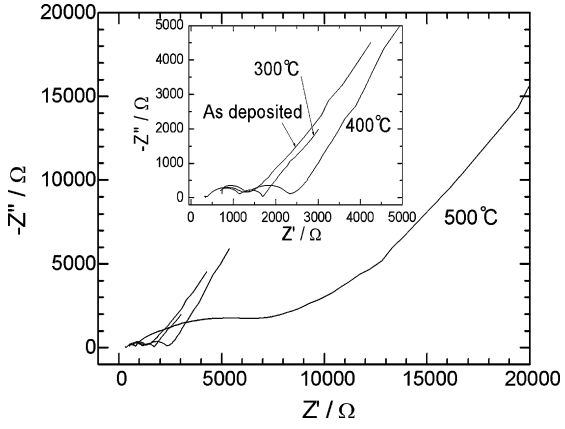

Fig. 4. Nyquist plots of Li/PEO/Ohara/$LiCoO_2$ cells measured at 50 °C.

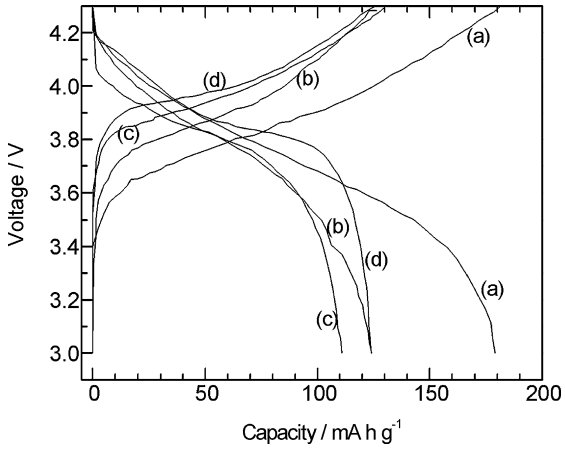

Fig. 5. Charge and discharge curves of Li/PEO/Ohara/$LiCoO_2$ cells at 50 °C at different annealing temperatures: (a) as-deposited, (b) 300 °C, (c) 400 °C and (d) 500 °C.

In the Li/PEO/Li cell, the high-frequency semicircle at room temperature is contributed by the PEO buck resistance, which was confirmed by the impedance of the Au/PEO/Au cell shown in Fig. 7. The low-frequency semicircle may be due to the Li/PEO interfacial resistance. From these results, the high-frequency semicircle and the low-frequency one in the Li/PEO/Ohara/PEO/Li cell correspond to the Li/PEO and the PEO/Ohara interfacial resistance, respectively. The resistance of Ohara was measured with the Au/Ohara/Au cell and it is about 300 Ω at room temperature as shown in Fig. 8, thus, the PEO/Ohara resistance is mainly due to the PEO/Ohara interfacial resistance. At 50 °C, the PEO/Ohara interfacial resistance is

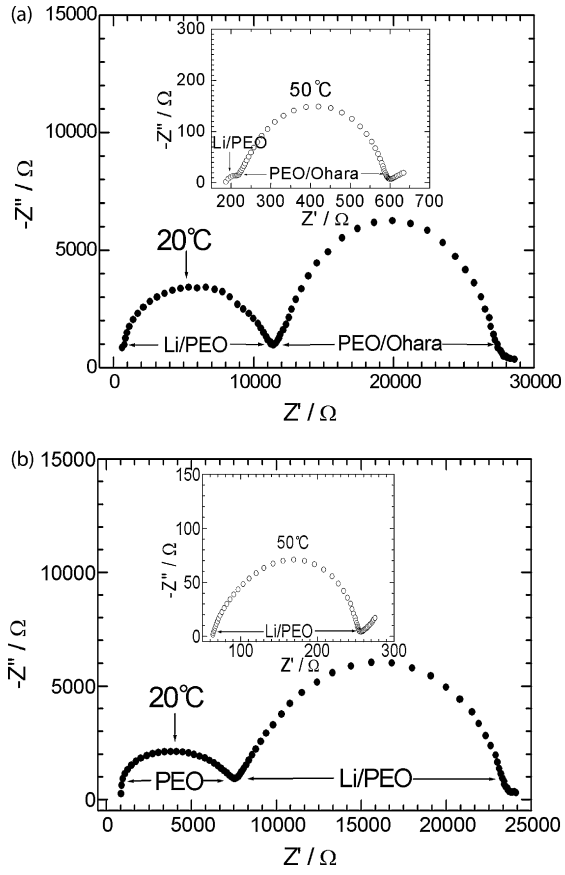

Fig. 6. Nyquist plots of symmetric cells: (a) Li/PEO/Ohara/PEO/Li and (b) Li/PEO/Li.

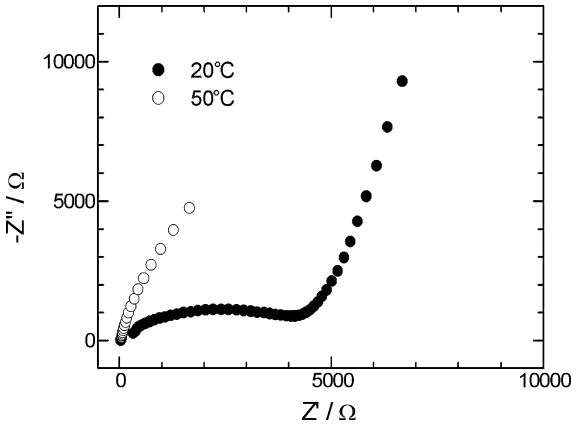

Fig. 7. Nyquist plots of symmetric cell Au/PEO/Au.

drastically decreased as seen in Fig. 6. It can be seen from Figs. 7 and 8, the bulk resistances of PEO and Ohara are neglectable compared with those of Li/PEO and PEO/Ohara interfacial resistance at 50 °C. Note that the resistance of Ohara bulk show slight changes before and after annealing at 700 °C for 30 min as shown in Fig. 8.

Fig. 9 shows the CV plots of the Li/PEO/Ohara/$LiCoO_2$ cells at 50 °C. The peaks, which correspond to the Li-ion intercalation/de-intercalation into/from $LiCoO_2$, become sharper with increasing annealing temperature. It may be due to the improved crystallization of $LiCoO_2$ film upon annealing. However, for the sample

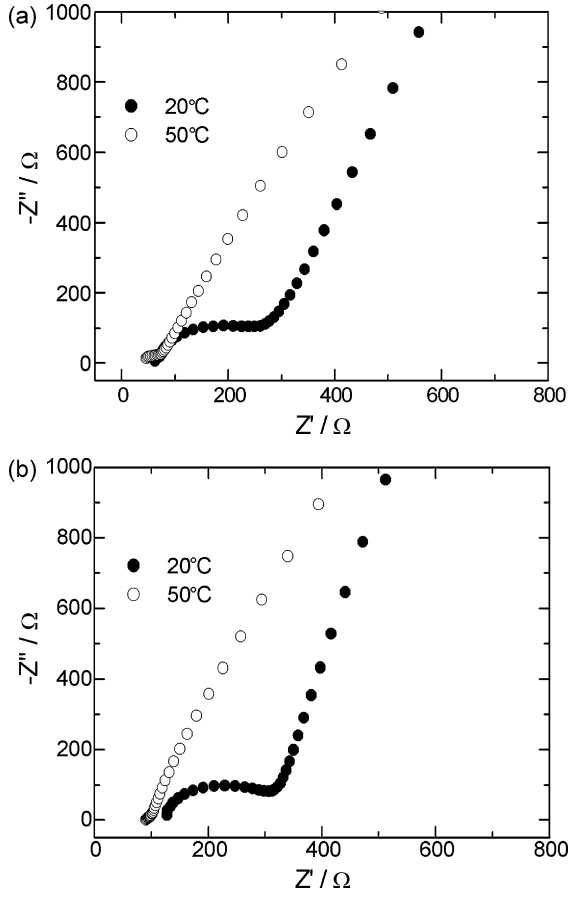

Fig. 8. Nyquist plots of symmetric cell Au/Ohara/Au: (a) as-assembled and (b) annealed at 700 °C for 30 min.

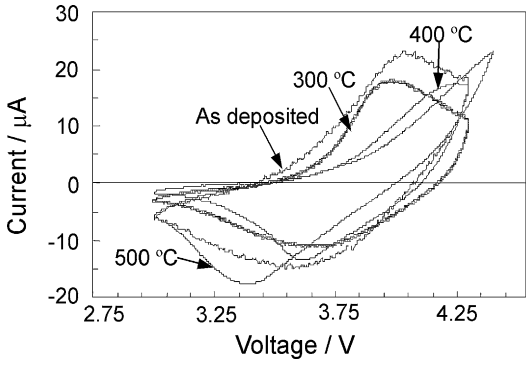

Fig. 9. CV plots of Li/PEO/Ohara/$LiCoO_2$ cells at 50 °C at different annealing temperatures.

annealed at 500 °C, the cathodic peak is shifted to the low potential and anodic one is not observed until 4.3 V vs. Li/Li^+. This result is due to a large polarization by the formation of the electrochemically inert Co_3O_4 phase in the Ohara/$LiCoO_2$ interface.

As observed above, the Li/PEO interfacial resistance, and PEO and Ohara bulk resistance are not so high compared with the PEO/Ohara interfacial resistance at 50 °C. The interfacial resistance has been more precisely studied. Fig. 10 shows typical Nyquist plots of the Li/PEO/Ohara/$LiCoO_2$ cell at various electrode potentials, where Ohara/$LiCoO_2$ was annealed at 400 °C for 30 min. The Nyquist plot is composed of a small semicircle in a high-frequency range, a large semicircle in a medium-frequency range and a sloping line in the low-frequency range. The high-frequency small semicircle, as clearly shown in the inset of Fig. 10, is attributed to the PEO/Ohara interfacial resistance. The diameter of the small semicircle shows a slight change with the increasing electrode potential. The large semicircle may correspond to the Li-ion transfer through Ohara/$LiCoO_2$ interface, which is on the increase with the increasing electrode potential. Fig. 11 compares the impedance spectra between the full cell Li/PEO/Ohara/$LiCoO_2$/Au at open circuit voltage and the symmetric cell Au/$LiCoO_2$/Ohara/$LiCoO_2$/Au at 50 °C. The results prove that the low-frequency semicircle in Fig. 10 is due to the Li-ion diffusion in the Ohara/$LiCoO_2$ interface. Fig. 12 shows the potential dependence of Li-ion transfer resistance, R_{ct}, through Ohara/$LiCoO_2$ interface at 50 °C. Note that the Li-ion transfer resistance increases with increasing annealing temperature of the Ohara/$LiCoO_2$ couple, especially that annealed at 500 °C. The increase of interfacial resistance is ascribed to the

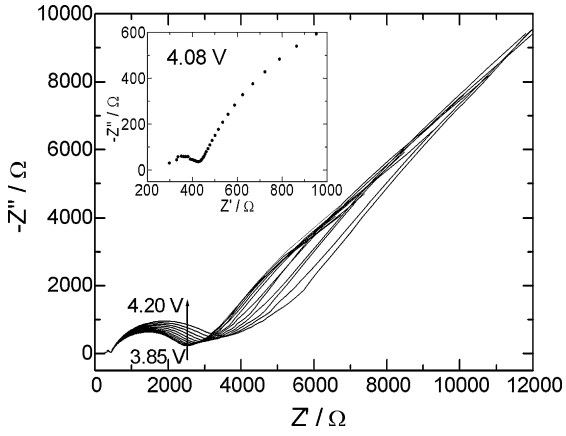

Fig. 10. Nyquist plots of Li/PEO/Ohara/$LiCoO_2$ cell at various electrode potentials using Ohara/$LiCoO_2$ annealed at 400 °C. The inset shows the Nyquist plot polarized at 4.08 V in the high-frequency range.

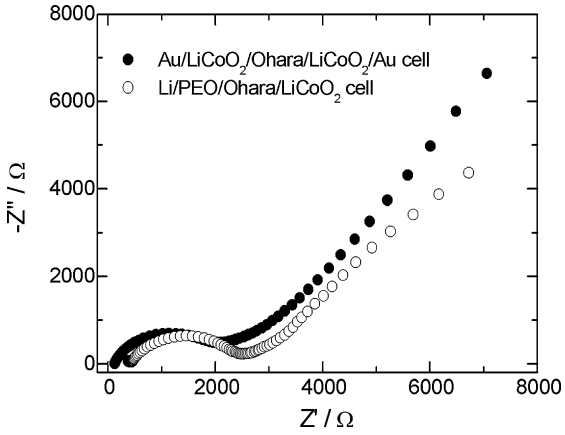

Fig. 11. Comparison of Nyquist plots between the full cell Li/PEO/Ohara/$LiCoO_2$/Au at open circuit voltage and the symmetric cell Au/$LiCoO_2$/Ohara/$LiCoO_2$/Au at 50 °C.

formation of the Co_3O_4 layer at elevated annealing temperature. The interfacial resistance of the Ohara/$LiCoO_2$ annealed at 300 °C and the as-deposited one show small change with the electrode potential, while it shows a gradual rise for the sample annealed at 400 °C and a sharp rise for the sample annealed at 500 °C, indicating that it becomes more difficult for Li-ion to transfer through the Ohara/$LiCoO_2$ interface containing Co_3O_4 at a low Li content in $Li_{1-x}CoO_2$. The interfacial resistance of Ohara/$LiCoO_2$ annealed at 400 °C is comparable with those of Ohara/$LiMn_2O_4$ and Ohara/$Li_4Ti_5O_{12}$ annealed at 600 °C [6,7].

In addition to the Ohara/$LiCoO_2$ interface, the Li-ion diffusion in $LiCoO_2$ bulk also plays an important role in the electrochemical performance of the Li/PEO/Ohara/$LiCoO_2$ cell. Therefore, Li-ion chemical diffusion coefficient of $Li_{1-x}CoO_2$ sputtered on Ohara, $\tilde{D}_{Li}$, was measured using PITT and EIS methods proposed by Huggins et al. [15,16]. The details for the measurement were described in [11]. In this study, the lithium ion conducting solid electrolyte,

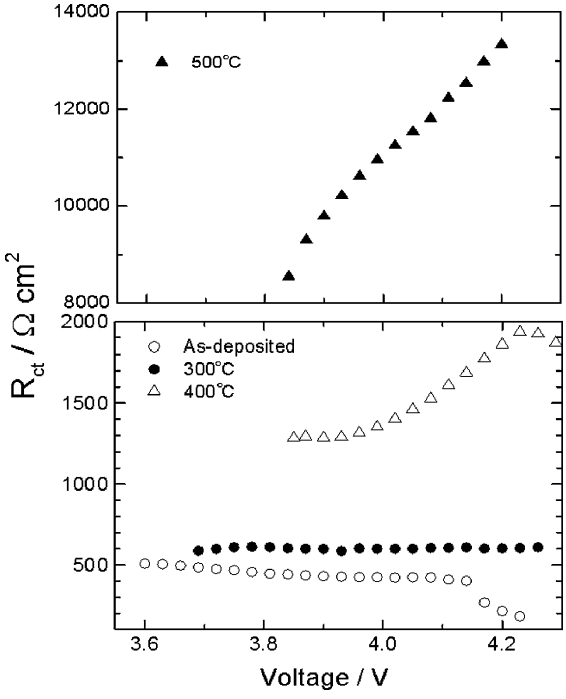

Fig. 12. Potential dependence of Li-ion transfer resistance through Li/PEO and Ohara/$LiCoO_2$ interfaces annealed at different temperatures.

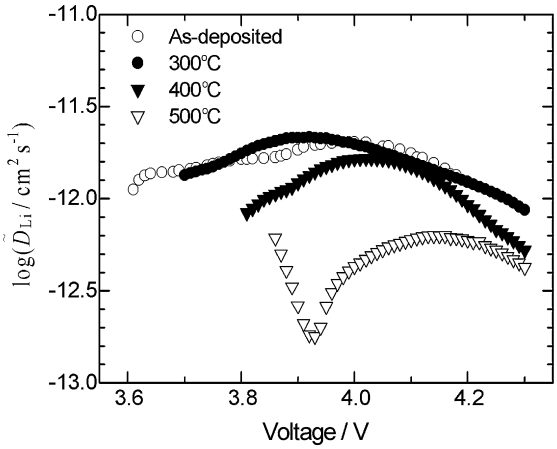

Fig. 13. Potential dependence of Li-ion chemical diffusion coefficients in $LiCoO_2$ thin films annealed at different temperatures measured by PITT.

Ohara, was used instead of the liquid electrolytes. Fig. 13 shows the potential dependence of Li-ion chemical diffusion coefficient in $Li_{1-x}CoO_2$ thin film annealed at different temperatures measured by PITT. Note that the $\tilde{D}_{Li}$ values for the as-sputtered and 300 °C annealed $Li_{1-x}CoO_2$ show no clear dependence on the electrode potential in amorphous $Li_{1-x}CoO_2$ lattice. The films annealed at higher temperatures show clearer dependence of $\tilde{D}_{Li}$ on the electrode potential as observed in the $Li_{1-x}CoO_2$ film on Au annealed at 700 °C [11]. As shown in Fig. 13, a maximum of $\tilde{D}_{Li}$ value is observed. The maximum is associated with the order/disorder transition near the composition $Li_{0.5}CoO_2$, where the degree of Li vacancy ordering is increased [17]. It is interesting to note that the potential, at which the maximum $\tilde{D}_{Li}$ value occurs, shifts to a large x value (high potential) in $Li_{1-x}CoO_2$ with increasing annealing temperature. It was reported that for the well-crystallized $LiCoO_2$ thin films, the maximum of $\tilde{D}_{Li}$ value appears at around 4. 15 V (or $x = 0.5$ in $Li_{1-x}CoO_2$) [17–19], which is close to our 500 °C annealed sample. The $\tilde{D}_{Li}$ values of the poorly crystallized $LiCoO_2$ thin films (as-deposited, annealed at 300 and 400 °C) range from 2.5×10^{-12} to 5×10^{-13} $cm^2\,s^{-1}$. The film annealed at 500 °C shows $\tilde{D}_{Li}$ values of 2 to 6.3×10^{-13} $cm^2\,s^{-1}$, which are one order smaller than those reported by us previously [11] and two orders smaller than those reported by Xia and Lu [19], which were measured with liquid electrolytes for (1 0 4) oriented films by PITT. These high diffusion coefficients may be due to the fact that the penetration of liquid electrolyte into electrode may facilitate the Li-ion diffusion. Li-ion

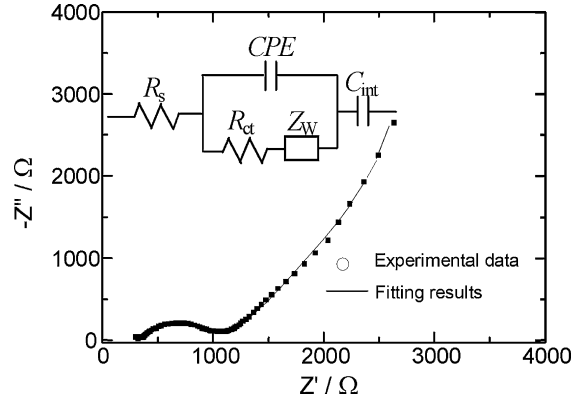

Fig. 14. A typical Nyquist plot at 4.05 V for the cell using as-deposited $LiCoO_2$ on Ohara. The inset shows the equivalent circuit for the fitting.

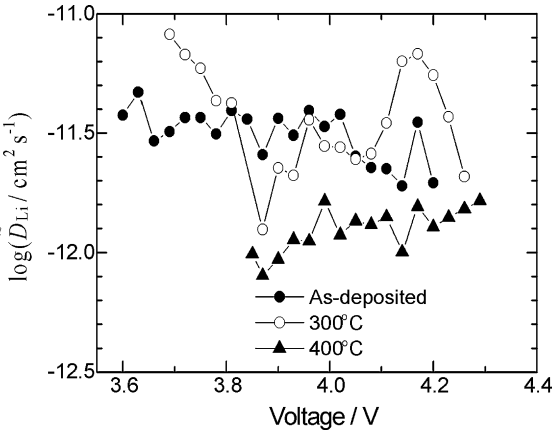

Fig. 15. Potential dependence of Li-ion chemical diffusion coefficients in $LiCoO_2$ thin films annealed at different temperatures measured by EIS.

diffusion in $Li_{1-x}CoO_2$ bulk may also be limited by the inert Co_3O_4 layer.

The chemical diffusion coefficient was also measured by EIS. Fig. 14 gives a typical Nyquist plot at 4.05 V for the Li/PEO/Ohara/as-deposited $LiCoO_2$ cell. The plot was fitted using the equivalent circuit shown in the inset. The calculation method of $\tilde{D}_{Li}$ values using EIS can refer to [11]. Fig. 15 shows the potential dependence of Li-ion chemical diffusion coefficient of $Li_{1-x}CoO_2$ using EIS. The $\tilde{D}_{Li}$ values of the poorly crystallized $LiCoO_2$ thin films range from 1×10^{-12} to 1×10^{-11} $cm^2\ s^{-1}$, which are comparable with that by Wang et al. [20] for the amorphous $LiCoO_2$ measured with Lipon electrolyte using EIS. We cannot obtain the $\tilde{D}_{Li}$ values using EIS for the $LiCoO_2$ thin film annealed at 500 °C due to the poorly developed impedance spectra in the low-frequency Warburg region. Wang et al. [20] observed a rise of $\tilde{D}_{Li}$ value by two orders of magnitude when the $LiCoO_2$ thin film transforms from an amorphous to the well crystalline state measured by EIS using Lipon as an electrolyte.

For the as-deposited and 300 °C annealed $LiCoO_2$ thin film, the Li-ion chemical diffusion coefficients in these films are in a range of 10^{-11} to 10^{-12} $cm^2\ s^{-1}$ at 50 °C. The total cell resistance of the Li/PEO/Ohara/$LiCoO_2$ cell was about 500 Ω cm^2, therefore, the IR drop at 1 mA cm^{-2} was about 0.5 V. With the increasing annealing temperature, the IR drop will become significant and the cell cannot tolerate large current density. The limiting current density, I_l, controlled by the Li-ion chemical diffusion in $LiCoO_2$ could be estimated from the following equation:

$$\tilde{D}_{Li} = \frac{I_l L}{FC}, \quad (1)$$

where L is the thickness of $LiCoO_2$, F the faraday constant and C the Li-ion concentration in $LiCoO_2$. The liming current density for the as-deposited and 300 °C $LiCoO_2$ thin films of 0.8 μm thickness is about 6×10^{-1} mA cm^{-2} for $\tilde{D}_{Li} = 10^{-11}$ $cm^2\ s^{-1}$ and 6×10^{-2} mA cm^{-2} for $\tilde{D}_{Li} = 10^{-12}$ $cm^2\ s^{-1}$. From above analyses, it seems that the cell performance was limited by the Li-ion diffusion resistance in Ohara/$LiCoO_2$ interface as well as in bulk $LiCoO_2$.

4. Conclusions

$LiCoO_2$ thin films deposited on Ohara by RF magnetron sputtering exhibited a (1 0 4) preferred orientation. Interfacial reaction between $LiCoO_2$ and Ohara occurs at 500 °C to form Co_3O_4. The interfacial resistance of Ohara/$LiCoO_2$ and the Li-ion chemical diffusion coefficient in $Li_{1-x}CoO_2$ were evaluated using the Li/PEO/Ohara/$LiCoO_2$ cells. It was found that the formation of Co_3O_4 layer hinders the Li-ion transfer in a voltage range 3–4.3 V. The Co_3O_4 layer not only blocks the Li-ion diffusion through Ohara/$LiCoO_2$ interface, but also limits the Li-ion transfer within the $LiCoO_2$ bulk. The interfacial resistance of Ohara/$LiCoO_2$ was below 2000 Ω cm^2 when it was annealed below 400 °C. By annealing at 500 °C it increased to over 8000 Ω cm^2. Li-ion chemical diffusion coefficient in the $LiCoO_2$ bulk ranges from 2.5×10^{-12} to 5×10^{-13} $cm^2\ s^{-1}$ by PITT and from 1×10^{-11} to 1×10^{-12} $cm^2\ s^{-1}$ by EIS when annealed below 400 °C. The $LiCoO_2$ film annealed at 500 °C shows low $\tilde{D}_{Li}$ values. The $\tilde{D}_{Li}$ values by EIS showed similar dependence on annealing temperature with those by PITT. The Li-ion diffusion resistance through Ohara/$LiCoO_2$ interface as well as $LiCoO_2$ bulk is the limiting factors in determining the electrochemical performance of the Li/PEO/Ohara/$LiCoO_2$ cell.

Acknowledgements

We thank OHARA Inc. for supplying the glass ceramics plates and are grateful to Dr. Y. Inda of OHARA Inc. for the helpful comments and suggestions. This research work was carried out under a collaboration program of Mie University and Genesis Research Institute, Nagoya, Japan.

References

[1] J. Fu, Solid State Ionics 96 (1997) 195.
[2] J. Fu, J. Am. Ceram. Soc. 80 (1997) 1901.
[3] P. Birke, F. Salam, S. Döring, W. Weppner, Solid State Ionics 118 (1999) 149.
[4] Y. Inda, T. Katoh, M. Baba, J. Power Sources 174 (2007) 741.
[5] Y. Iriyama, C. Yada, T. Abe, Z. Ogumi, K. Kikuchi, Electrochem. Commun. 8 (2006) 1287.
[6] K. Dokko, K. Hoshina, H. Nakano, K. Kanamura, J. Power Sources 174 (2007) 1100.
[7] K. Hoshina, K. Dokko, K. Kanamura, J. Electrochem. Soc. 152 (2005) A2138.
[8] K. Nagata, T. Nanno, J. Power Sources 174 (2007) 832.
[9] Q. Li, H.Y. Sun, Y. Takeda, N. Imanishi, J. Yang, O. Yamamoto, J. Power Sources 94 (2001) 201.
[10] J. Xie, N. Imanishi, T. Matsumura, A. Hirano, Y. Takeda, O. Yamamoto, Solid State Ionics 179 (2008) 362.
[11] J. Xie, N. Imanishi, A. Hirano, T. Matsumura, Y. Takeda, O. Yamamoto, Solid State Ionics 178 (2007) 1218.
[12] C. Julien, M.A. Camacho-Lopez, L. Escobar-Alarcon, E. Haro-Poniatowski, Mater. Chem. Phys. 68 (2001) 210.
[13] C.L. Liao, K.Z. Fung, J. Power Sources 128 (2004) 263.
[14] S.B. Tang, M.O. Lai, L. Lu, J. Alloys Compd. 424 (2006) 342.
[15] C.J. Wen, B.A. Boukamp, R.A. Huggins, W. Weppner, J. Electrochem. Soc. 126 (1979) 2258.
[16] C. Ho, I.D. Raistrick, R.A. Huggins, J. Electrochem. Soc. 127 (1980) 345.
[17] Y.I. Jang, B.J. Neudecker, N.J. Dudney, Electrochem. Solid-State Lett. 4 (2001) A74.
[18] H. Xia, L. Lu, G. Ceder, J. Power Sources 159 (2006) 159.
[19] H. Xia, L. Lu, Electrochim. Acta 52 (2007) 7014.
[20] B. Wang, J.B. Bates, F.X. Hart, B.C. Sales, R.A. Zuhr, J.D. Robertson, J. Electrochem. Soc. 143 (1996) 3203.